Accepted Manuscript

Petroleum Geoscience

Radioactive Heat Production variations in the Faroe-Shetland Basin: key new heat production, geological and geochronological data for regional and local basin modelling

Alexander J Finlay, David S. Wray, Guy Comfort & Julian K Moore

DOI: https://doi.org/10.1144/petgeo2022-039

To access the most recent version of this article, please click the DOI URL in the line above. When citing this article please include the above DOI.

This article is part of the UKCS Atlantic Margin collection available at: https://www.lyellcollection.org/topic/collections/new-learning-from-exploration-and-development-in-the-ukcs-atlantic-margin

Received 20 May 2022
Revised 3 April 2023
Accepted 2 August 2023

Supplementary material at https://doi.org/10.6084/m9.figshare.c.6771540

Radioactive Heat Production variations in the Faroe-Shetland Basin: key new heat production, geological and geochronological data for regional and local basin modelling.

Alexander J Finlay[1] , David S. Wray[2], Guy Comfort[1] & Julian K Moore[3]

[1]Chemostrat Ltd, 1 Ravenscroft Court, Buttington Enterprise Park, Welshpool, SY21 8SL, UK
alexfinlay@chemostrat.com
[2]School of Science, Faculty of Engineering & Science, University of Greenwich, Chatham Maritime, Kent, ME4 4TB, UK.
[3]APT Ltd, Unit 8, Tan-y-Graig, Parc Caer Seion, Conwy, LL32 8FA,UK

Abstract:
This study presents the results of a joint Chemostrat – APT study that aimed to produce a suite of Radioactive Heat Production (RHP) data for basement rocks in the Faroe Shetland Basin to enable more accurate basin modelling to be undertaken. To enable regional studies to be undertaken, the basement has been split into four zones based on similarities. Zone A is formed of high grade metamorphic basement from the Rockall trough (quads 154 & 164) southwest of the "Laxfordian front" postulated by Holdsworth et al., (2019). Zone B comprises granodioritic, tonalitic and dioritic Neoarchean aged (2700-2830 Ma) high grade metamorphic basement from the southwest of the Rona Ridge and Basin (wells 202/08-1, 204/15-2, 205/161, 205/21-1A, 206/7a-2, 206/08-2, 206/09-2 and 206/12-1) and northeast of the Laxfordian front. Zone C contains Neoarchean aged high grade metamorphic basement of a predominantly granitic and quartz rich granitoid composition from the northeast of the Rona Ridge (wells 207/01-3, 207/02-1, 208/23-1 and 208/26-1). Zone D differs from the rest of the material in this study in that it is Caledonian (~460 Ma) granitic plutonic basement from Quads 209 (Ereland volcanic centre). Radioactive heat production values were derived from Potassium, Thorium and Uranium data produced from the analysis of eighty-four basement samples by ICP-OES and ICP-MS analysis. Each mapped basement zone was then assigned a mean radioactive heat production value for use in future basin modelling studies; Zone A = 0.21 μWm^3, Zone B, 0.64 μWm^3, zone C = 0.88 μWm^3 and zone D = 2.1 μWm^3.

Historically, petroleum system analysis in the Faroe Shetland Basin (FSB) has always struggled to match results with the observed geology. For example all published basin modelling studies report 'early' (Cretaceous) generation for the Faroe-Shetland basin (e.g. Iliffe et al. 1999; Holms et al. 1999; Mark et al. 2005) and the OGA petroleum systems chart for the West of Shetland and West of Hebrides, released as part of the 32nd licencing round, places the 'critical moment' for oil generation in the Mid to Late Cretaceous, before common Palaeogene reservoirs such as the Lamba and Vaila sands are deposited. Several explanations have been put forward to try and explain this mismatch between observed geology and modelled results, such as oil migrating into deeper holding reservoirs before re-migrating into the Palaeocene (e.g. the motel model; Lamer and Carmichael 1999) or overpressure retarding the expulsion of oil from source rock (e.g. Carr & Scotchman, 2003).

These published petroleum systems analysis studies do not account for all aspects of the petroleum system, one of particular relevance to the Faroe-Shetland basin is the variation in radioactive heat production (RHP) from basement. A focussed study around the Corona ridge demonstrated that basement here is "old and cold" (Gardiner et al. 2019) with basement RHP values averaging ~1.6 µW/m3, significantly lower than the default values of upper-crust RHP in most basin modelling software (e.g., set at ~2.8–3.2 µW/m3 in Genesis and PetroMod). By using these colder RHP values, Gardiner et al. (2019) produced a basin model that estimated oil generation and expulsion around the Corona Ridge in the Palaeogene, after the deposition of local reservoirs. This model invoked a combination of reduced RHP in the Crust together with section thickening associated with Paleogene intrusions; a corollary of the latter is the decreased conductivity of the total section. The selection of ~1.6 µW/m^3 in Gardiner et al. 2019 was somewhat pragmatic. Despite the importance of an appropriate selection of the RHP parameter in basin models, there exists very limited data and studies on the degree to which the RHP may vary within a basin.

This paper seeks to understand variations in basement RHP across the FSB at both the local and regional level to enable accurate petroleum system modelling to be undertaken. Local RHP data has been produces for wells 154/03-1, 164/25-2, 202/02-1, 202/03-1, 202/08-1, 202/09-1, 204/10-1, 204/15-2, 204/23-1, 204/25-1, 205/16-1, 205/20-1, 205/21-1A, 205/22-1A, 206/08-1A, 206/08-2, 206/08-7, 206/08-8, 206/09-2, 206/12-1, 206/7a-2, 207/01-3, 207/02-1, 208/23-1, 208/26-1, 208/27-2, 209/09-1, 209/12-1, 214/09-1 and 220/26-1. Regional RHP values have been calculated for four different zones in the FSB. These zones have been assigned due to similarities/differences in their minerology, texture and geochronology.

Crystalline basement in the Faroe-Shetland Basin

The geology of the Faroe-Shetland basin has been studied in detail by Chambers et al. (2005), Ritchie et al. (2011) and Holdsworth et al. (2019). Mapping basement in the FSB is difficult due to irregular basement penetration from oil and gas well cover. However, Holdsworth et al., (2019) suggest that the metamorphic basement should be viewed as a single "Faroe-Shetland" Terrane linked to the Rae Craton of East Greenland (Fig. 1a). This terrane is predominantly made up of upper amphibolite (and possibly granulite) facies granodioritic gneisses with lesser abundances of more granitic, intermediate, and mafic gneiss material (Holdsworth et al., 2019). Uranium – Lead dating of zircons from these units demonstrate that their igneous protoliths crystalised in the Neoarchean (2729-2826 Ma, Holdsworth et al., 2019; 2700-2829 Ma, Chambers et al., 2005). This terrane is bounded to the south west by an

approximately positioned limit to Laxfordian reworking, dividing it from the Lewisian complex of Scotland and the Nagssugtoqidian of Greenland (fig. 1a; Holdsworth et al., 2019). In addition to the high grade metamorphic basement of the Faroe-Shetland Terrane, there are four volcanic centres to the North East of the basin (Brendan, Erlend, Franeir and West Erlend) which are thought to be Palaeogene (e.g. fig. 1 of Layfield et al., 2022). The main north east to south west striking structure in the basin (fig 1b) were formed by thrusts during the Caledonian orogeny and normal faults during the Devonian Orogenic collapse and Permian to Cenozoic extension, forming the intrabasinal ridges (see Layfield et al., 2022 and references therein).

Sample material and methods

For this study, new elemental, mineralogical and U-Pb zircon analysis has been undertaken (Fig. 2 and Table 1) and a literature search was conducted providing historical Elemental data (Chemostrat multiclient report: NE129, Chambers et al., 2005 & Finlay et al., 2018), U-Pb zircon geochronology (Ritchie et al., 2011, Chemostrat, 2014 & Holdsworth et al., 2019) and Petrology (Chambers et al., 2005, Finlay et al., 2018 & Holdsworth et al., 2019; Table 2). This enabled sufficient data to be collected to calculate the RHP of 85 samples (Table 3).

Potassium (K), Thorium (Th) and Uranium (U) elemental data, utilised for Radioactive Heat Production calculations (RHP; Turcotte and Schubert, 2014) was either collected from the published literature or generated from new analysis as part of this study at Origin Analytical Ltd (table 1). Each sample was washed and dried to remove any surface mud and/or contaminants. Prior to analysis, all prepped cuttings samples were then ground to a fine powder in agate mortars. Following preparation, the cuttings samples were prepared for ICP analyses by using the lithium metaborate (alkali) fusion procedure, as advocated by Jarvis & Jarvis (1992a and 1992b). The prepared samples were then analysed using ICP-OES and ICP-MS instruments, with quantitative data being acquired for forty-eight elements, which include ten major elements, e.g., Al, Si, Ti, Fe, Mn, Mg, Ca, Na, K and P, twenty-four trace elements, e.g., Ba, Be, Co, Cr, Cs, Cu, Ga, Hf, Mo, Nb, Ni, Pb, Rb, Sc, Sr, Ta, Tl, Th, U, V, W, Y, Zn and Zr, and fourteen rare earth elements, e.g., La, Ce, Pr, Nd, Sm, Eu, Gd, Tb, Dy, Ho, Er, Tm, Yb and Lu. The precision of the geochemical data acquired by the ICP analyses is determined by replicate analyses of multiple preparations of certified rock standard reference materials (SRMs), along with duplicate preparations of three unknown samples, which are analysed on a routine basis along with each of the samples. With reference to the SRMs, the absolute accuracy of all the data are generally considered to lie within the range of error achieved for multi-determinations of the same sample.

In addition to producing RHP data for individual sample for local petroleum system analysis, mineralogical and geochronological data was used to investigate if the basement could be split into discrete zones based on changes in geology and geochronology.

For core material, mineralogical data was collected through point counting of 300 crystals from a thin section by Chemostrat Ltd. In addition, the texture of the thin section (metamorphic grade or igneous characteristic) was recorded.

For XRD analysis of cuttings material, samples were disaggregated prior to micronizing using a McCrone mill using propan-2-ol as the liquid phase to minimise loss of water-soluble phases. Samples were then sieved and side mounted into sample holders to maintain a random orientation of the grains. X-ray diffraction analysis was performed with a Siemens D5000 diffractometer using CoKα radiation (35kV, 35mA) and a scan range from 2 to 80°2θ. Mineral identification was undertaken using the Bruker Eva® software package and the ICDD crystallographic database. Quantification was performed using an in-house modification of the Rockjock® software package (Eberl, 2003), with confirmation of the clay mineral phases derived from a separate, oriented sample of the clay phases, investigated air dried, glycolated, and heated to 400 & 550°C

Uranium-Lead dating was undertaken on zircons separated from Basement samples. Zircon grains were separated using LST heavy mineral separation at Origin Analytical Ltd and then analysed by laser ablation inductively-coupled plasma mass spectrometry (LA-ICP-MS) at the University of Greenwich. The nonmagnetic fraction (>1.2A) was mounted in araldite resin blocks and polished. The resin blocks were then placed into a Scanning Electron Microscope (SEM) and mapped using electron dispersive spectroscopy to identify zircons in the sample using zirconium abundance to identify the zircons and elevated Hf abundance to confirm. U-Pb age dating was performed using quadrupole-based LA-ICP-MS. Mass bias and instrument drift were monitored constantly and accounted for by using sample standard bracketing. Zircon isotopic standard 91500 (Weidenbeck *et al.,* 1995 & 2004) was used as the primary calibration standard and the calibration was validated using the Plešovice zircon isotope standard (Sláma *et al.,* 2008) run as an unknown. Raw data were processed using Iolite v3 software (Patton et al. 2011). All analytical errors in the text are quoted at 2 σ level. All zircon analyses were displayed on concordia diagrams (Vermeesch, 2012; Fig. 5) to check the data for any major peculiarities and for geologically significant discordia arrays. The single analysis concordia age (op. cit.) was calculated for each analysis and these ages were used for plotting and interpreting the data. This age has the advantage of being more precise than both the 206Pb/207Pb ages and the 206Pb/238U ages (Zimmermann et al., 2017) and therefore removes the need to switch between isotope systems at a given age (typically 1.0 Ga).

Results and discussion

Localised Radioactive Heat Production

Radioactive heat production data has been produced for both new elemental analyses carried out in this study (n=55), or data found in the literature (Chambers et al., 2005; n=20 and Finlay et al., 2018 n=11). This was undertaken using the method of Turcotte and Schubert (2014) and an assumed density of 2700Kg m-3 (the same as utilised in Gardiner et al., 2019). Mean RHP values have then been calculated for each well samples in this study (Table 3; fig. 3). Generally, RHP for wells in the Faroe-Shetland Terrane (wells from quads 154, to 208; Fig. 1 and 2) possess values ranging from 0.01 to 1 µWm-3, with a gradual rise in RHP from SW to NE. Wells 209/09-1 and 214/09-1 lie to the North East of the Faroe Shetland Terrane, with well 209/09-1 in the Erlend Volcanic centre, and possess higher RHP values of ~1.8 to 2.6 µWm3.

Regional Radioactive Heat Production

To produce regional RHP data, wells need to be clumped into zones based on their likely RHP characteristics. Radioactive heat production is primarily driven by the radioactive decay of K, Th and U. The abundance of these elements in geological samples is controlled by two variables:

1. The age of a rock – as older rocks have undergone increased amounts of radioactive decay reducing the amount of radioactive parent material.
2. The mineralogical content of the rock - radioactive elements (e.g K and U) are dominantly found in Feldspars and Clays (K) and zircons (U) respectively (e.g Salminen et al., 2005).

Minerology and rock type

This study therefore utilises minerology and U-Pb geochronology to split the basement in the FSB into discrete RHP zones.

Mineralogical data (Table 4) was utilised to classify each analysed sample based on its quartz, alkali feldspar and plagioclase feldspar composition (Streckeisen, 1967, Fig 4). This new data (n=37) combined with data from the literature (thin sections descriptions; Chambers et al., 2005, n=16; and Holdsworth et al., 2019, n=9; and QAP designation, Finlay et al., 2018, n=10) produced a new rock type database of 72 samples. Full point count and XRD data is available in table SI1.

These results are as expected from what has previously been reported for the FSB, with the textural data either being metamorphic (wells from quads 202-208) or plutonic (wells from quad 209). This enables us to split these samples into two separate basement zones. Wells 209/09-1, 209/12-1 and 241/09-1 form a plutonic zone and the rest of the wells to the south east form a metamorphic zone.

When the samples that have a metamorphic texture are plotted by themselves, two sperate groups of data appear. In the north east of the basin, wells 207/01-3, 207/02-1, 208/23-1 and 208/26-1 are predominantly granitic and quartz rich granitoid, with minor granodiorite and no tonalitic or dioritic material in composition. In the south west of the basin, wells 202/08-1, 204/15-2, 205/161, 205/21-1A, 206/7a-2, 206/08-2, 206/09-2 and 206/12-1 are dominated by granodioritic, tonalitic and dioritic material with minor granitic samples. This suggests that there is a lithological change across the metamorphic basement enabling it to be subdivided into two separate zones.

U-Pb zircon geochronology

U-Pb zircon geochronology was undertaken on twelve samples of which one did not contain enough zircons to produce an age (Table 5). Ages were based on the upper intercept of a Wetherill Discordia diagram (Fig. 5; green filled elapses) produced in isoplot R (Vermeesch, 2012). The 2sd the uncertainty in the age was taken using the "y" uncertainty in isoplotR (approximate 100(1-α)% confidence interval for t with overdispersion, calculated as $z = y\sqrt{MSWD}$ (only reported if MSWD > 1). Full U-Pb zircon data are available in table SI2.

In addition to this new data produced in this study, data has been collected from Ritchie et al. (2011; n=1), Chemostrat (2014, n=4) and Holdsworth et al. (2019; n= 12). The method used for collecting data by Chemostrat (2014) and the new U-Pb zircon ages in this study differs from that used by Holdsworth et al. (2019) in that no CL imaging was undertaken to establish if the core of a zircon had

been analysed, due to the method being developed for high throughput commercial, rather than academic, analysis. Instead, the centre of each separated grain has been targeted. Furthermore, analysis has been undertaken on amalgamated depths of drill cuttings for well 204/10-1 (8219-8248'), 205/16-1 (14108-14154') and 207/01-2 (4670-4706'). Analysing drill cuttings has the inherent risk that caved material from younger lithologies from higher up the well may be inadvertently analysed. To try and minimise this risk, careful screening of the cuttings was undertaken to remove any obviously caved material. Both of these changes from standard methodology mean that the results produced in this study need to be checked before being accepted. This has been undertaken in three ways.

Firstly, three samples were collected from over ~1m of core from well 207/02-1 (6722', 6723' and 6724'; fig 6a). If the method utilised by this study was not rigorous enough to produce valid geochronological data, it would be expected that the ages from these three samples would have a large uncertainty, vary significantly and not agree with previously reported data from the basin. However, the ages produced are all precise and agree within uncertainty (2732 ± 4 Ma; 2735 ± 5 Ma and 2735 ± 4 Ma respectively). Furthermore, these ages are all well within that expected in the basin (2700-2830 Ma; Holdsworth et al., 2019). Secondly, both basement cuttings and core samples were collected from well 205/16-1 (core 14027' and cuttings 14108-14154'). If the cuttings were contaminated by caved material then again they would not be expected to produce a precise age in agreement to that produced from core and other sourced in the basin. However, the data produced is both precise and in agreement between the two samples (cutting age 2742 ± 6 Ma; core age 2738 ± 6 Ma; fig 6b) and other data produced from the basin. It is noted that the other cutting sample utilised in this study did produce an age of reduced precision (well 207/01-3, depth 4670-4706', age 2734 ± 16 Ma), however it is still an age as expected in the basin, therefore it is suggested that this reflects some internal sample heterogeneity rather than caved material. Thirdly, all the data in this study has been compared to that previously published for the basin (fig. 6c) is all within the 2700-2830 Ma age window for the basin produced by Holdsworth et al. (2019). Therefore, we are confident in the data produced in this study.

The ages from this study and the published data show that the two metamorphic zones split by their minerology are indistinguishable geochronologically and so may not be separate mappable units. However, for the purposes of calculating RHP, their different minerology will affect their chemical make-up and so are still used to produce separate regional RHP data.

In addition to the metamorphic basement, a sample of plutonic material from well 209/09-1 produced an age of 463 ± 6 Ma. This demonstrates that the Erlend volcanic centre from the NE of the basin is in fact Caledonian, not Palaeogene in Origin.

Zoning of basement for calculating regional RHP in the FSB and links with basement geology

Based on the data produced in this study, combined with the published data four zones have been established for producing regional RHP data in the FSB (Fig. 7).

- Zone A. Metamorphic basement from the Rockall trough (quads 154 & 164) southwest of the "Laxfordian front" postulated by Holdsworth et al., (2019)

- Zone B. Metamorphic basement from the southwest of the Rona Ridge and Basin (wells 202/08-1, 204/15-2, 205/161, 205/21-1A, 206/7a-2, 206/08-2, 206/09-2 and 206/12-1), NE of the "Laxfordian front" postulated by Holdsworth et al., (2019). Neoarchean aged material (2700-2830 Ma) dominated by Granodioritic, tonalitic and dioritic material.
- Zone C. Metamorphic basement from the North East of the Rona Ridge (wells 207/01-3, 207/02-1, 208/23-1 and 208/26-1). Neoarchean aged material (2700-2830 Ma) dominated by predominantly Granitic and Qtz rich granitoid material.
- Zone D. Caledonian plutonic basement from Quads 209 (Erland volcanic centre).

Regional Radioactive Heat Production (RHP) in the FSB

Using the new RHP zoning produced by this study, four new regional RHB vales are suggested for future basin models in the FSB. These show a warming from the coldest in the southwest, warming to the northeast (Fig. 8). Median and Mean RHP data for each mapped zone are:

- Zone A
  Median RHP – 0.2 μWm3
  Mean RHP – 0.2 μWm3
  SD – NA
  N – 2 (As zone A only has two RHP data and therefore these low values may just be a result of under sampling)
- Zone B
  Median RHP – 0.64 μWm3
  Mean RHP – 0.78 μWm3
  SD – 0.58
  N - 51
- Zone C
  Median RHP - 0.88 μWm3
  Mean RHP – 0.89 μWm3
  SD – 0.45
  N - 20
- Zone D
  Median RHP – 2.1 μWm3
  Mean RHP -2.1 μWm3
  SD - 0.66
  N - 12

This expanded study supports the conclusions of Gardiner et al. (2019) that the Neoarchean basement is "old and cold" with an Average RHP value of ~0.9 μW/m3 and so default RHP values set at ~2.8–3.2 μW/m3 in Genesis and PetroMod cannot be used in the FSB. However, Caledonian aged granitic material in the northeast of the basin is much warmer (~2.1 μW/m3), although still cooler than default Genesis and PetroMod values. These cold basement RHP values may help therefore explain the postulated mismatch seen between petroleum generation ages in the published literature (e.g. Lamers and Carmichael 1999). Importantly for basin modelling, each of the basement zones identified in this study also have different RHP values, ranging from coolest in the Southwest to warmest in the

Northeast (fig. 4). Therefore, it is important that basin modelling work carried out in the FSB does not assume a single RHP value.

Gardiner et al. 2019 concluded that after using a cooler RHP (1.6 μW/m3) and including ~1.1km of Paleogene intrusive material in a pseudo-well located in a basial area of the FSB that oil generation still initiated in the Cretaceous, implying additional processes must be considered to predict the 'critical moment'. The value of the 'critical moment' as a concept was reviewed by Moore & He (2021). In the deeper parts of the basin where the Jurassic is over 7 km deep present-day, irrespective of the thermal (or pressure) model invoked, maturation will be early relative to the deposition of reservoirs and seals. Evidence of earlier charge phases exists in fluid inclusion data e.g., Mark *et al*. (2005) and isotopic data (e.g. Holdsworth et al. 2019; Finlay et al. 2011). The principal issue is not the occurrence of early generation but the adherence to the 'critical moment' concept and its importance in petroleum system analyses (Moore & He, 2021). While a full analysis of the controlling aspects of the petroleum system are beyond the scope of this paper, they appear to include cool crust as discussed in this work and in addition: basin geometries, trap and seal behaviour (cf. Sales, 1997) and migration lag (cf. Moore & He, 2021).

The importance of appropriate RHP parameterisation and hence temperature prediction in sedimentary basins also has implications for any process that requires temperature prediction away from well control, such as diagenetic modelling for reservoir quality prediction, reservoir biodegradation risk and many aspects of well planning (cement design; petrophysical tool selection etc).

Geological controls on RHP in the FSB and future work.

As stated above, these zones have been defined to enable the production of regional RHP values. However, there is evidence that these zones may be driven by the geological history of the FSB. Only two basement samples have been analysed for RHP in Zone A and so any inferences about this zone must be treated with caution. These samples differ from the rest of this study in that are very cold (H=~0.2) and are sourced from the Rockall trough, southwest of the Laxfordian front (Holdsworth et al., 2019) and associated with Lewisian basement complex basement, rather than that of the Faroe-Shetland Terrane (Fig. 1). Could this terrane be generally colder than that of the FSB, perhaps due to Laxfordian (1.7-1.8 Ga) alteration mobilising and removing radioactive elements? Future analysis of material onshore Lewisian (Scotland) and Nagssugtoqidian (Greenland) material would confirm this.

Radioactive Heat Production zones B and C both lie within the Faroe Shetland Terrane, however it is noticeable that zone B is coincident with the Lancaster and Grater Clair sub area and Zone C the Victory sub area of Holdsworth et al. (2019). The different regional RHP values from this study should be applied to different models in these areas. Zone C is also sited in the northeast of the Faroe Shetland Terrane, close to a possible continuation of the Caledonian Moine Thrust. Could the more felsic composition of this zone be related to the Caledonian orogeny, for example fluid flow, or is it just natural variation? Detailed descriptions of thin sections from this area as carried out by Holdsworth et al., (2019) may help answer this but was outside the scope of this work. Furthermore, apatites have been separated from the heavy mineral fractions utilised in this study and are currently undergoing

U-Pb dating. Apatite has a lower closure temperature (375-600 C; Kirkland et al., 2018) than zircons and so may be reset to Caledonian ages if this event has effected these wells.

Zone D has the highest RHP data produced in this study and the plutonic basement from well 209/9-1 in the Erlend Volcanic Centre which is clearly Caledonian in age, not Palaeogene as previously suggested (e.g. Layfield et al., 2022). The RHP data from the other plutonic rocks in the zone are similar to those produced by Caledonian plutonic basement from the Utsira High and Lake District (RHP = 2.1, SD = 2.7, n=15; Finlay, 2019), and cooler than those of Palaeogene granites from Ireland (RHP = 7.5, SD = 4, n= 4; Finlay et al., 2019). It seems likely that the majority of granites in this area are Caledonian in age rather Paleogene, and so the Caledonian front may lie to the southwest of this zone. As above, further geochronology is being undertaken on these samples to try and confirm this.

Conclusions

This paper presents new Radioactive Heat Production data for individual basement samples, averaged by well and regionally across the Faroe-Shetland Basin. Radioactive Heat Production ranges from ~0.1 to 1.4 µWm3 across the Faroe Shetland Terrane and generally rises from southwest to northeast. Northeast of the Faroe Shetland Terrane RHP are higher (~1.6-2.4 µWm3). The basement has been split into four sperate zones based on variations in their minerology and geochronology, and each assigned a RHP value for regional basin modelling studies. Zones A-C represent Neoarchean metamorphic basement and zone D Caledonian granitic basement. Generally, the basin is colder in the southwest and warmer in the northeast:

Zone A. RHP = 0.2 µWm3.
Metamorphic basement from the Rockall trough (quads 154 & 164) southwest of the "Laxfordian front" postulated by Holdsworth et al., (2019)
Zone B. RHP = 0.64 µWm3.
Metamorphic basement from the south west of the Rona Ridge and Basin (wells 202/08-1, 204/15-2, 205/161, 205/21-1A, 206/7a-2, 206/08-2, 206/09-2 and 206/12-1), NE of the "Laxfordian front" postulated by Holdsworth et al., (2019). Neoarchean aged material (2700-2830 Ma) dominated by Granodioritic, tonalitic and dioritic material.
Zone C. RHP = 0.88 µWm3.
Metamorphic basement from the North East of the Rona Ridge (wells 207/01-3, 207/02-1, 208/23-1 and 208/26-1). Neoarchean aged material (2700-2830 Ma) dominated by predominantly Granitic and Qtz rich granitoid material.
Zone D. RHP = 2.1 µWm3.
Caledonian plutonic basement from Quads 209 (Erland volcanic centre).

Acknowledgements
Prof. Rob Strachan is thanked thanked for his comments and suggestions that aided production of this paper. The authors with to acknowledge Prof. Bob Holdsworth and one anonymous reviewer for their constructive comments that have greatly aided the production of this paper. Chemostrat Ltd and APT Ltd are also thanked for enabling publication of the new data in this paper.

References

Carr, A. D., & Scotchman, I. C. (2003). Thermal history modelling in the southern Faroe–Shetland Basin. *Petroleum Geoscience*, *9*(4), 333-345.

Chambers, L., Darbyshire, F., Noble, S., & Ritchie, D. (2005). NW UK continental margin: chronology and isotope geochemistry.

Chemostrat multiclient study: NE129, Chemostratigraphy of the Palaeocene, U.K. Rockall Basin

Chemostrat report, 2014. Dating West of Shetland basement using U-Pb Zircon ages: A reconnaissance study.

Eberl, D.D. 2003. User's guide to RockJock -- a program for determining quantitative mineralogy from powder x-ray diffraction data. USGS Open-File Report 03-78, 48pp.

Finlay, A.J., Carr, A., Hedley, B., Holt, B., O'Neil, P., Gardner, D., & Darling, J., 2018. Calculated radioactive heat production from basement & sediments: Implications for basin & petroleum system modelling. PETEX, London.

Finlay, A.J. 2019 Calculated radioactive heat production in the North Sea: new data for petroleum systems analysis. Petroleum Systems Analysis 'Science or Art?' conference, London.

Gardiner, D., Schofield, N., Finlay, A., Mark, N., Holt, L., Grove, C., Forster, C. and Moore, J., 2019. Modelling petroleum expulsion in sedimentary basins: The importance of igneous intrusion timing and basement composition. Geology, 47(10), pp.904-908.

Holdsworth, R.E., Morton, A., Frei, D., Gerdes, A., Strachan, R.A., Dempsey, E., Warren, C. and Whitham, A., 2019. The nature and significance of the Faroe-Shetland Terrane: linking Archaean basement blocks across the North Atlantic. *Precambrian Research*, *321*, pp.154-171.

Holmes, A. J., Griffith, C. E., & Scotchman, I. C. (1999, January). The Jurassic petroleum system of the West of Britain Atlantic margin–an integration of tectonics, geochemistry and basin modelling. In *Geological Society, London, Petroleum Geology Conference Series* (Vol. 5, No. 1, pp. 1351-1365). Geological Society of London.

Iliffe, J. E., Robertson, A. G., Ward, G. H. F., Wynn, C., Pead, S. D. M., & Cameron, N. (1999, January). The importance of fluid pressures and migration to the hydrocarbon prospectivity of the Faeroe–Shetland White Zone. In *Geological Society, London, Petroleum Geology Conference Series* (Vol. 5, No. 1, pp. 601-611). Geological Society of London.

Jarvis, I., & Jarvis, K. E. (1992A). Inductively coupled plasma-atomic emission spectrometry in exploration geochemistry. *Journal of Geochemical Exploration*, *44*(1-3), 139-200.

Jarvis, I., & Jarvis, K. E. (1992B). Plasma spectrometry in the earth sciences: techniques, applications and future trends. *Chemical Geology*, *95*(1-2), 1-33.

Kirkland C.L. Yakymchuk, C., Szilas, K., Evans, N., Hollis, J., McDonald, B., Gardiner, N.J., 2018. Apatite: a U-Pb thermochronometer or geochronometer? Lithos, 318–319, 143-157

Lamers, E., & Carmichael, S. M. M. (1999, January). The Paleocene deepwater sandstone play West of Shetland. In *Geological Society, London, Petroleum Geology Conference series* (Vol. 5, No. 1, pp. 645-659). Geological Society of London.

Layfield, L.K., Schofield, N., Jolley, D.W., Holford, S.P., Volintir, T.R., Kilhams, B.A., Muirhead, D.K. and Cromie, H., 2022. New insights into the structure, geology and hydrocarbon prospectivity along the

central-northern Corona Ridge, Faroe–Shetland Basin. *Petroleum Geoscience*, *28*(4), pp.petgeo2021-090.

Mark, D. F., Parnell, J., Kelley, S. P., Lee, M., Sherlock, S. C., & Carr, A. (2005). Dating of multistage fluid flow in sandstones. *Science*, *309*(5743), 2048-2051.

Marshall, Daniel (1996), Ternplot: An Excel spreadsheet for Ternary diagrams, Computers and Geosciences, vol. 22 #6, p. 697-699.

Moore, J.K. & He, Z. 2021. The West of Shetland Petroleum System. GeoExpro, Vol. 18, No. 3. Available online at: https://www.geoexpro.com/articles/2021/06/the-west-of-shetland-petroleum-system

Paton, C., Hellstrom, J., Paul, B., Woodhead, J., & Hergt, J. (2011). Iolite: Freeware for the visualisation and processing of mass spectrometric data. *Journal of Analytical Atomic Spectrometry*, *26*(12), 2508-2518.

Ritchie, J. D., & Hitchen, K. (1996). Early Paleogene offshore igneous activity to the northwest of the UK and its relationship to the North Atlantic Igneous Province. *Geological Society, London, Special Publications*, *101*(1), 63-78.

Ritchie, J.D., Noble, D., Darbyshire, F., Mllar, I., & Chambers, L., 2011. Pre-Devonian. BGS Research Report RR/11/01 In: Ritchie, J.D., Ziska, H., Johnson, H., Evans, D. (Eds.), Geology of the Faroe -Shetland Basin and Adjacent Areas, 71–78. Sales, 1997

Salminen R, Batista J, Bidovec M, Demetriades A, De Vivo B, De Vos W, Duris M, Gilucis A, Gregorauskiene V, Halamic J, Heitzmann P, Lima A, Jordan G, Klaver G, Klein P, Lis J, Locutura J, Marsina K, Mazreku A, O'Connor PJ, Olsson SÅ, Ottesen R-T, Petersell V, Plant JA, Reeder S, Salpeteur I, Sandstrom H, Siewers U, Steenfelt A, Tarvainen T. 2005. Part 1: Background information, methodology and maps. In Salminen R, ed, Geochemical Atlas of Europe. EruoGeoSurveys, Espoo, Finland.

Sircombe, K. N. (2004). AgeDisplay: an EXCEL workbook to evaluate and display univariate geochronological data using binned frequency histograms and probability density distributions. *Computers & Geosciences*, *30*(1), 21-31.

Sláma, J., Košler, J., Condon, D. J., Crowley, J. L., Gerdes, A., Hanchar, J. M., ... & Whitehouse, M. J. (2008). Plešovice zircon—a new natural reference material for U–Pb and Hf isotopic microanalysis. *Chemical Geology*, *249*(1-2), 1-35.

Streckeisen, A., 1967, Classification and nomenclature of igneous rocks. Nues Jarbuch fur Mineralogie Abhandlungen, v. 107, p. 144-240.

Turcotte, D. L. and Schubert, G.: Geodynamics, Cambridge University Press, Cambridge, UK., 2014

Vermeesch, P. (2012). On the visualisation of detrital age distributions. *Chemical Geology*, *312*, 190-194.

Wiedenbeck, M., Allé, P., Corfu, F., Griffin, W.L., Meier, M., Oberli, F., von Quadt, A., Roddick, J.C. and Spiegel, W. (1995). Three natural zircon standards for U-Th-Pb, Lu-Hf, trace element and REE analyses. Geostandards Newsletter, **19**, 1-23

Wiedenbeck, M., Hanchar, J.M., Peck, W.H., Sylvester, P., Valley, J., Whitehouse, M., Kronz, A., Morishita, Y., Nasdala, L., Fiebig, J., Franchi, I., Girard, J.-P., Greenwood, R.C., Hinton, R., Kita, N., Mason, P.R.D., Norman, M., Ogasawara, M., Piccoli., P.M. , Rhede, D., Satoh, H., Schulz-Dobrick, B., Skår, Ø., Spicuzza, M.J., Terada, K., Tindle, A., Togashi, S., Vennemann, T., Xie, Q. and Zheng, Y.-F.

(2004). Further characterisation of the 91500 zircon crystal. Geostandards and Geoanalytical Research, **28**, 9-39.
Zimmermann, S., Mark, C., Chew, D., & Voice, P. J. (2018). Maximising data and precision from detrital zircon U-Pb analysis by LA-ICPMS: The use of core-rim ages and the single-analysis concordia age. Sedimentary geology, 375, 5-13.

Tables

Table 1. Summary of well, depth and materials utilised for new data produced by this study.

Table 2. Summary data utilised from published literature.

Table 3. Elemental and Radioactive heat production data (RHP; Calculated following the method of Turcotte and Schubert 2014, using an assumed rock density of 2700 Kg/m3 as used by Gardiner 2019) for individual samples and averaged by well.

Table 4. Lithological determination of rock type for new data in this study and thin section descriptions for literature data.

Table 5. Summary of U-Pb zircon geochronological data produced by this and previous studies

Table SI1. Full point count and Xray diffraction data

Table SI2. Full U-Pb zircon results.

Figure Captions

Figure 1: Regional and basial geological maps of the study area (modified from Holdsworth et al., 2019 and Layfield et al., 2022).

Figure 2: Map showing wells where samples have been utilised in this study. Fig. 2A – wells utilised for Mineralogical analysis. Fig. 2B – Wells utilised for U-Pb zircon geochronology. Fig. 2C – Wells where samples have been analysed to produce Radioactive Heat Production data.

Figure 3: Mean Radioactive Heat Production (H) data for each well utilised in this study (Table 3). Uncertainty bars reflect 1sd variation in data.

Figure 4: Quartz, Alkali-Feldspar, Plagioclase Feldspar plots (Streckeisen, 1967) for (A) all new mineralogical data collected in this study (Table 4 and Table SI1), (B) wells from quad 207 and 208 dominated by Granitic material, and (C) other wells from the Faroe Shetland Basin dominated by Granodioritic-Tonalitic-Dioritic material. Plotted using Ternplot (Marshall 1996).

Figure 5: U-Pb zircon Discordia diagrams for all newly analysed samples in this study (Table 5 and Table SI2). Zircon accepted for the Discordia age are in green ellipses (2 sigma uncertainty) and those rejected have no fill. Plotted using IsoplotR (Vermeesch, 2012).

Figure 6: U-Pb zircon quality control plots comparing (A) three dates over ~1m of core, (B) A core and cutting sample from the same well, and (C) all data produced in this study to that from the published literature. Uncertainty bars are 2SD.

Figure 7: Comparison of (A) the basement zones utilised for producing regional RHP data in this study and (B) areas utilised by Holdsworth et al. (2019).

Figure 8: Average Radioactive Heat Production for each basin zone in this study.

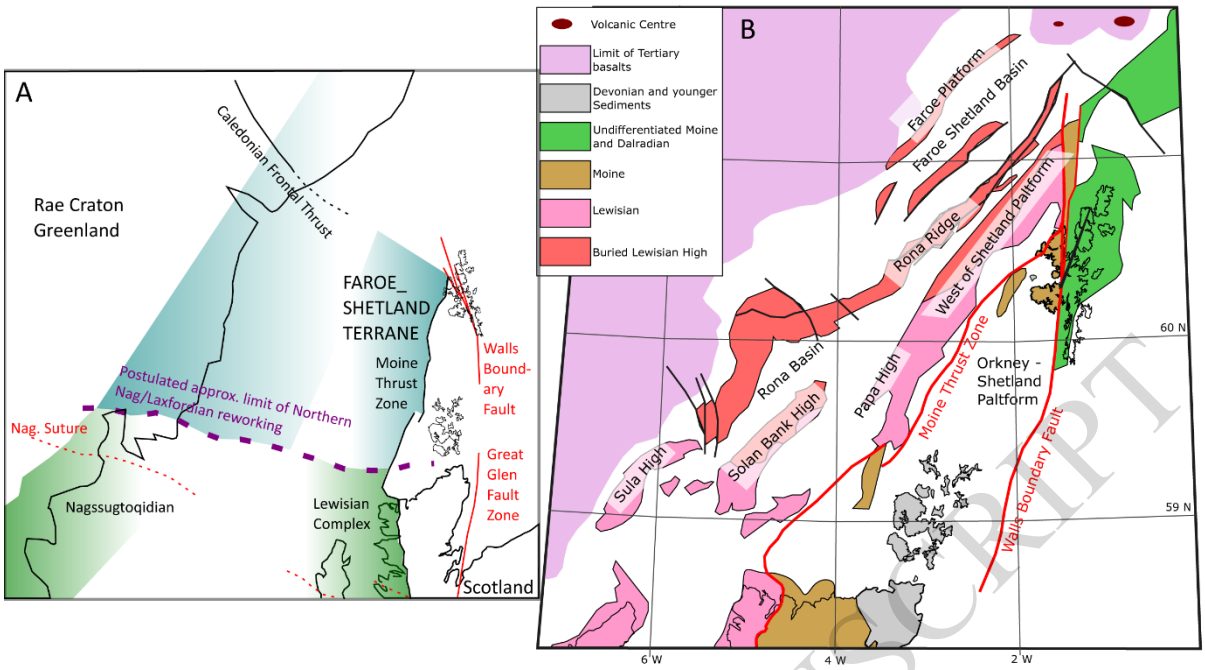

Figure 1

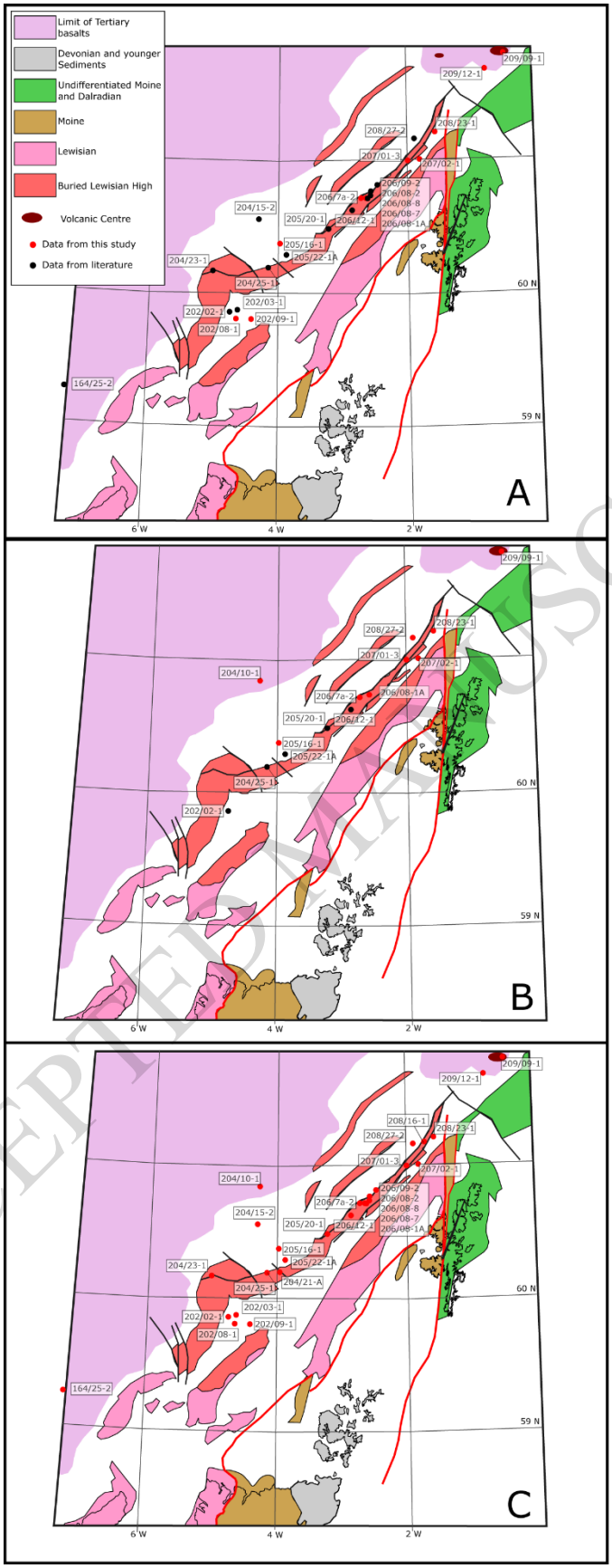

Figure 2

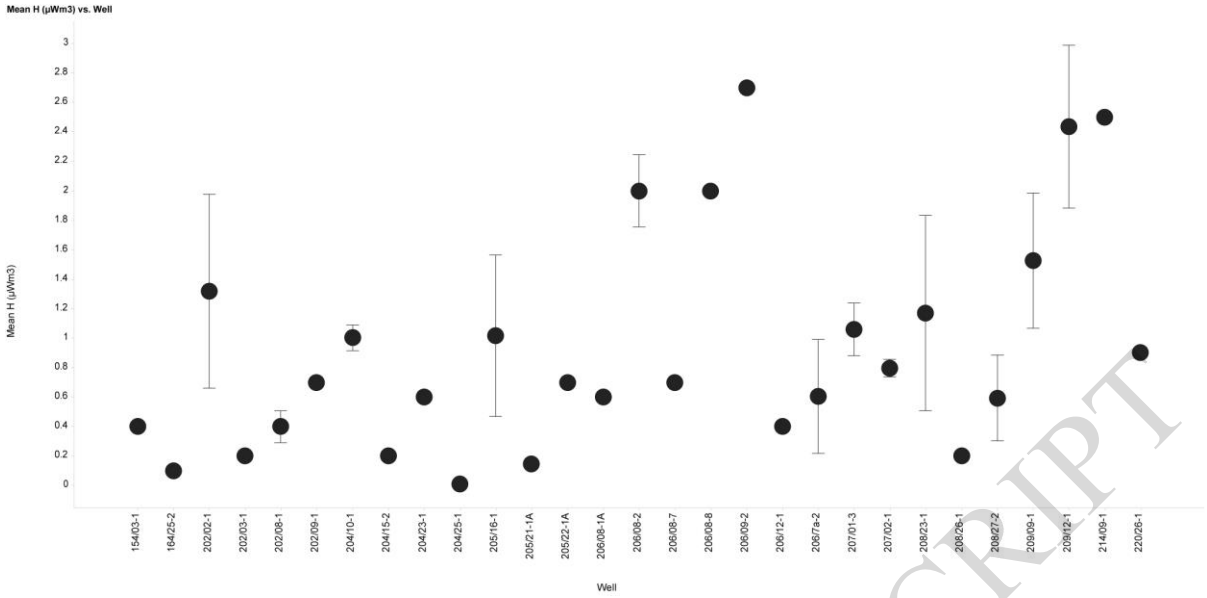

Figure 3

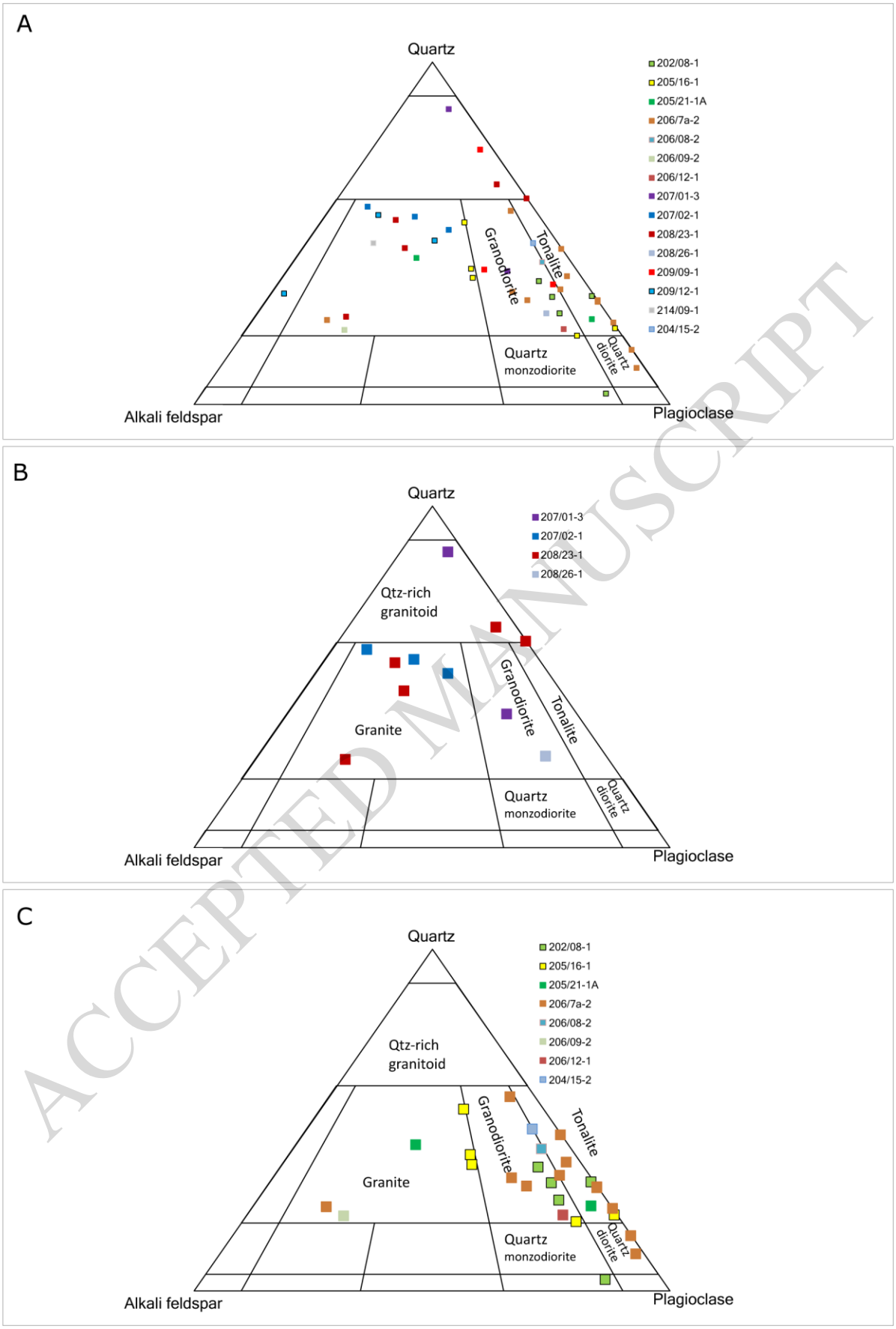

Figure 4

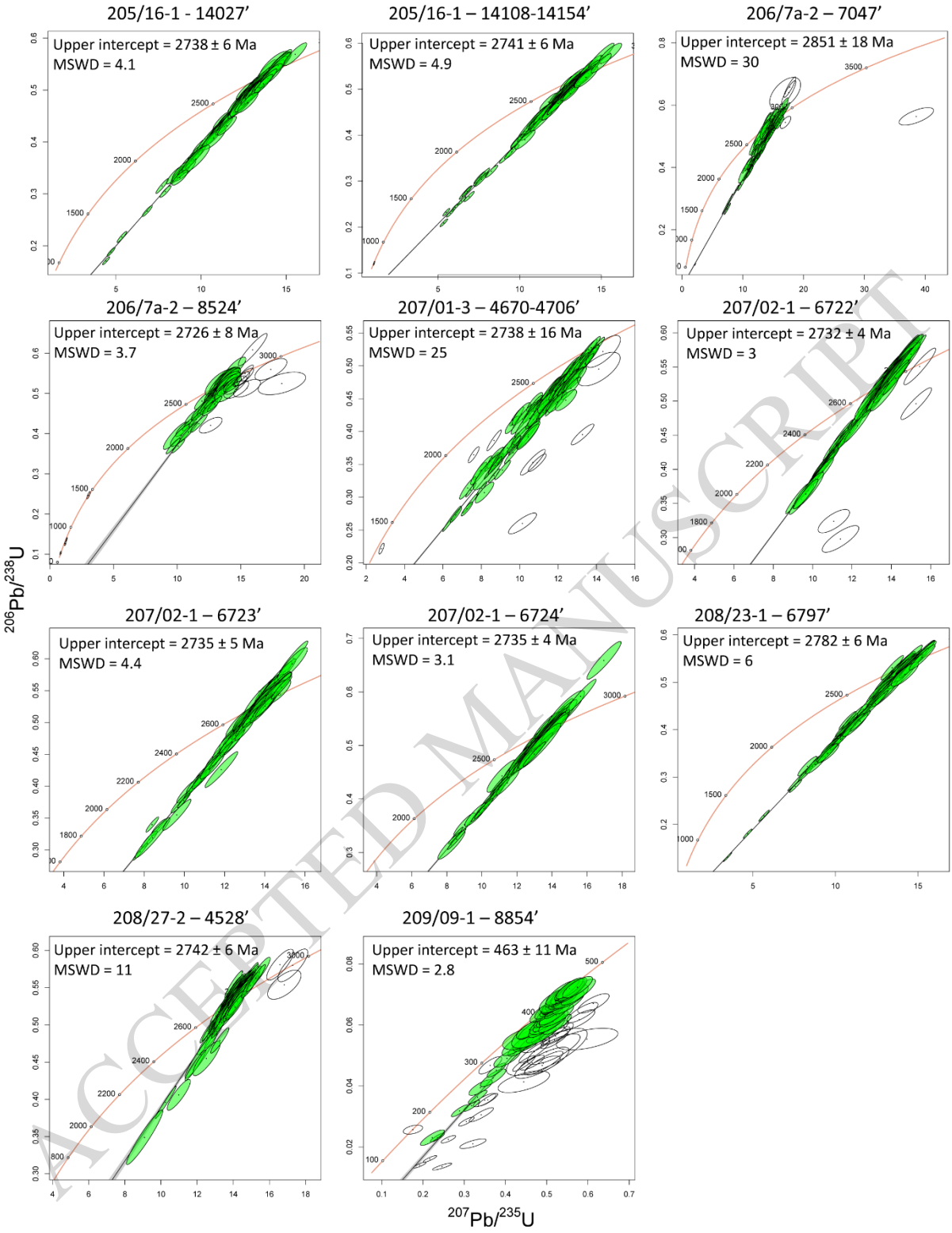

Figure 5

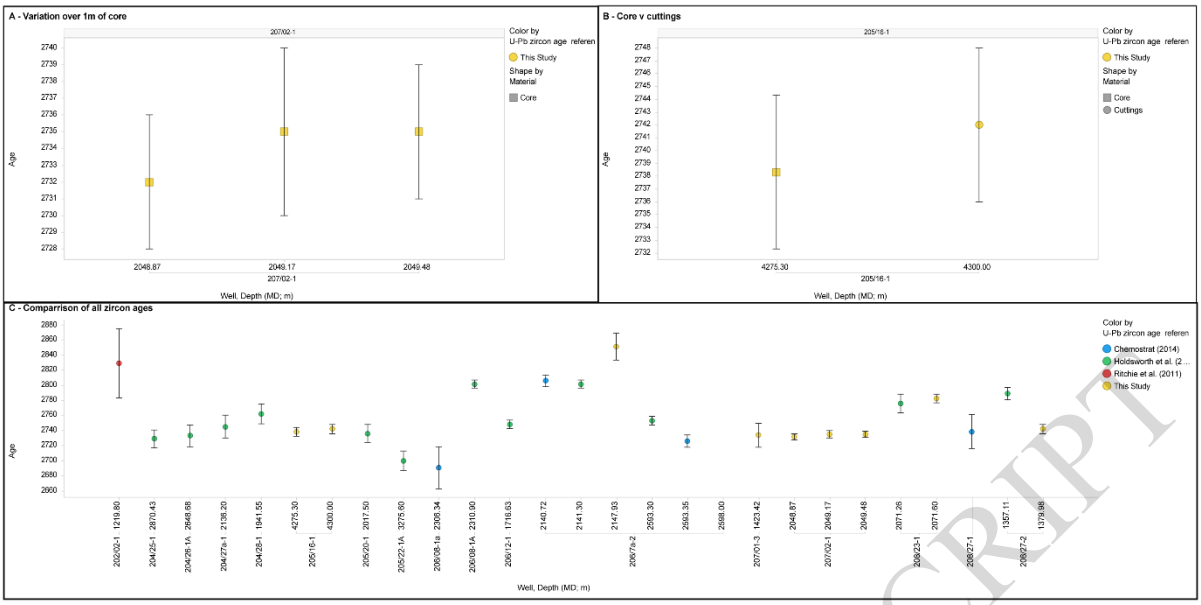

Figure 6

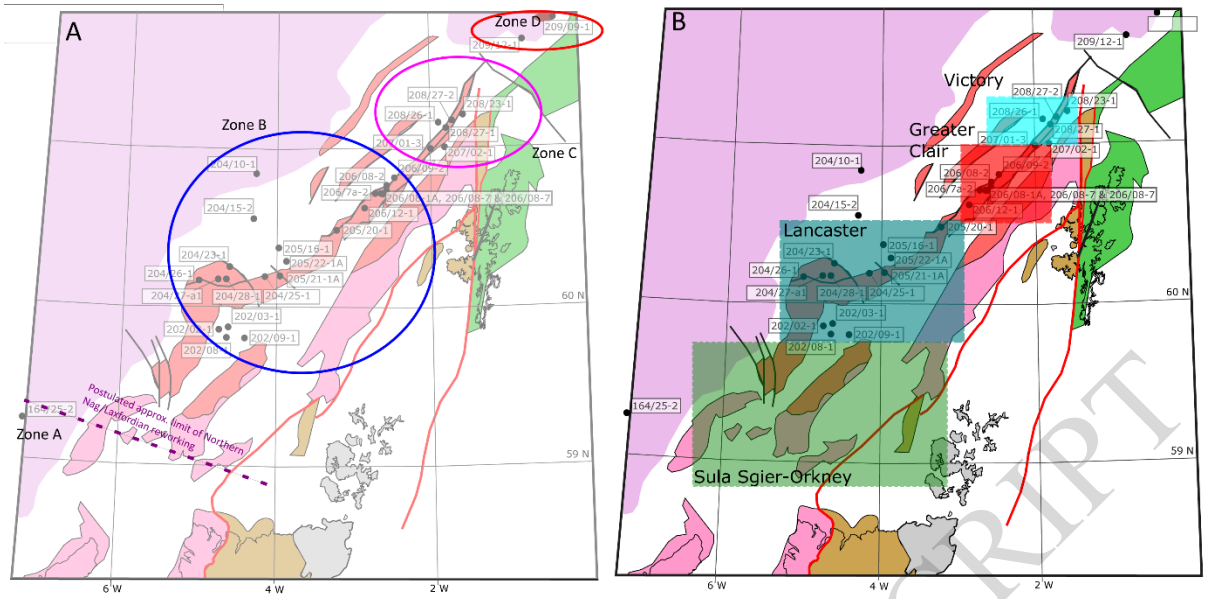

Figure 7

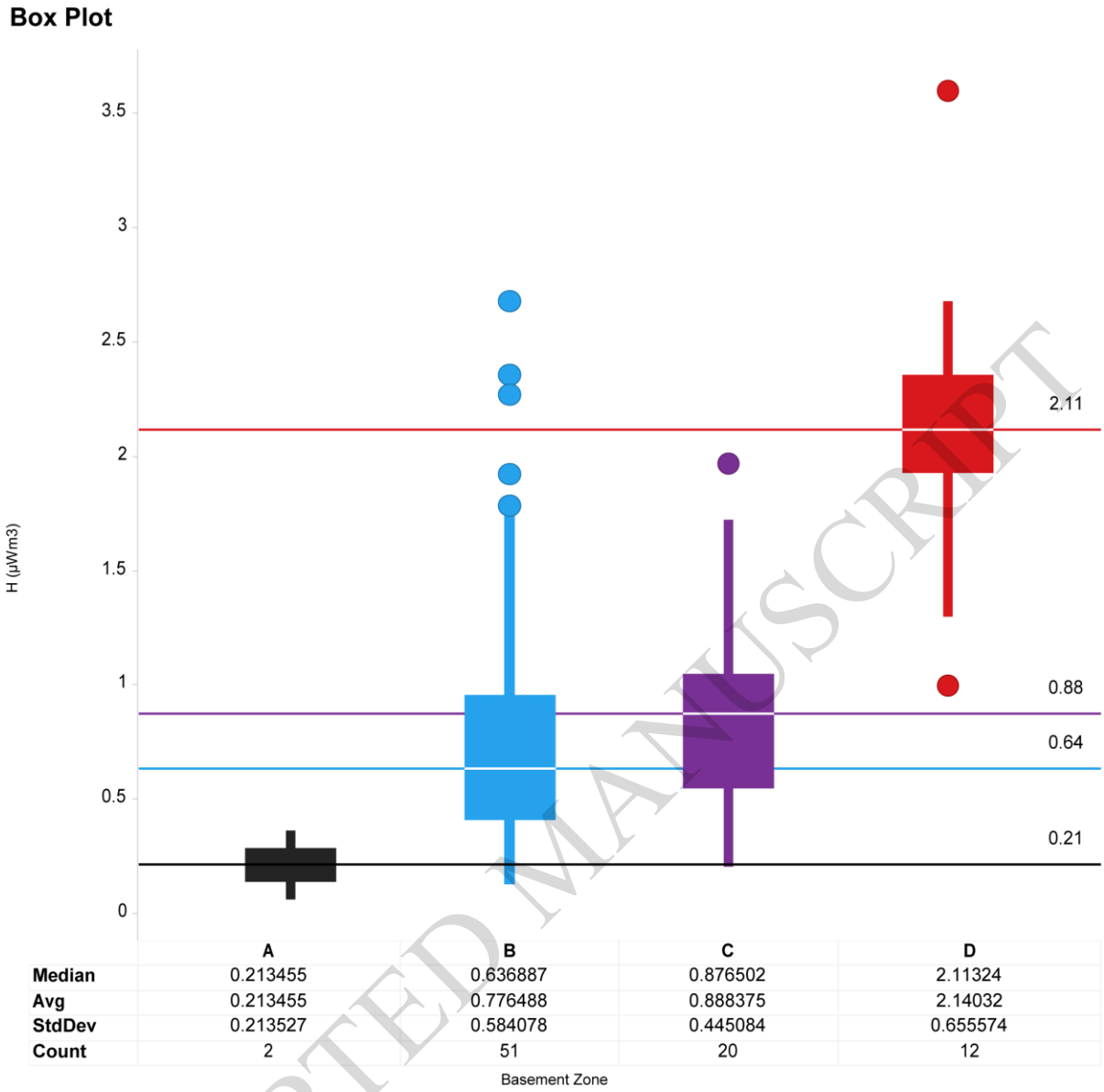

	A	B	C	D
Median	0.213455	0.636887	0.876502	2.11324
Avg	0.213455	0.776488	0.888375	2.14032
StdDev	0.213527	0.584078	0.445084	0.655574
Count	2	51	20	12

Figure 8

Table 1

Well	Depth	depth **m**	Sample material		Data type	
202/02-1	3950	1204.0	Cuttings			RHP
202/08-1	5447	1660.1	Core		Thin Section	RHP
202/08-1	5457	1663.4	Core		Thin Section	RHP
202/08-1	5500	1676.4	Cuttings		XRD	RHP
202/08-1	5510	1679.4	Cuttings		XRD	RHP
202/08-1	5520	1682.5	Cuttings		XRD	RHP
202/09-1	5379	1639.5	Core		Thin Section	RHP
204/10-1	8219	2505.0	Cuttings			RHP
204/10-1	8228	2508.0	Cuttings			RHP
204/10-1	8238	2511.0	Cuttings			RHP
204/10-1	8248	2514.0	Cuttings			RHP
205/16-1	14023	4274.4	Core		Thin Section	RHP
205/16-1	14024	4274.6	Core		Thin Section	RHP
205/16-1	14027	4275.3	Core	U-Pb zircon Age	Thin Section	RHP
205/16-1	14039	4279.2	Core		Thin Section	RHP
205/16-1	14108	4300.0	Cuttings			RHP
205/16-1	14124	4305.0	Cuttings	Amalgimated cuttings U-Pb zircon Age	Amalgimated cuttings XRD	RHP
205/16-1	14140	4310.0	Cuttings			RHP
205/16-1	14154	4314.0	Cuttings			RHP
206/7a-2	7043	2146.7	Core		Thin Section	RHP
206/7a-2	7047	2147.9	Core	U-Pb zircon Age	Thin Section	RHP
206/7a-2	7370	2246.4	Core		Thin Section	RHP
206/7a-2	8014	2442.6	Core		Thin Section	RHP
206/7a-2	8016	2443.2	Core		Thin Section	RHP
206/7a-2	8223	2506.5	Core		Thin Section	RHP
206/7a-2	8345	2543.7	Core		Thin Section	RHP
206/7a-2	8508	2593.3	Core		Thin Section	RHP
206/7a-2	8517	2596.0	Core		Thin Section	RHP
206/7a-2	8524	2598.0	Core	U-Pb zircon Age	Thin Section	
207/01-3	4576	1394.9	Core		Thin Section	RHP
207/01-3	4670	1423.4	Cuttings			RHP
207/01-3	4680	1426.5	Cuttings	Amalgimated cuttings U-Pb zircon Age	Amalgimated cuttings XRD	RHP
207/01-3	4690	1429.5	Cuttings			RHP
207/01-3	4700	1432.6	Cuttings			RHP
207/01-3	4706	1434.4	Cuttings			RHP
207/02-1	6722	2048.9	Core	U-Pb zircon Age	Thin Section	RHP
207/02-1	6723	2049.2	Core	U-Pb zircon Age	Thin Section	RHP
207/02-1	6724	2049.5	Core	U-Pb zircon Age	Thin Section	RHP
208/23-1	6797	2071.6	Core	U-Pb zircon Age	Thin Section	RHP

208/23-1	6799	2072.4	Core		Thin Section	RHP
208/23-1	6803	2073.6	Core		Thin Section	RHP
208/23-1	6806	2074.5	Core		Thin Section	RHP
208/23-1	6808	2075.1	Core		Thin Section	RHP
208/27-2	4522	1378.4	Core			RHP
208/27-2	4528	1380.0	Core	U-Pb zircon Age		RHP
208/27-2	4531	1381.1	Core			RHP
208/27-2	4532	1381.4	Core			RHP
209/09-1	8850	2697.5	Core		Thin Section	RHP
209/09-1	8854	2698.6	Core		Thin Section	RHP
209/09-1	8855	2698.9	Core	U-Pb zircon Age	Thin Section	RHP
209/12-1	11386	3470.4	Core			RHP
209/12-1	11500	3505.2	Cuttings			RHP
209/12-1	11510	3508.2	Cuttings		Amalgimated cuttings XRD	RHP
209/12-1	11520	3511.3	Cuttings			RHP
209/12-1	11525	3512.8	Core		Thin Section	RHP
209/12-1	11527	3513.4	Core		Thin Section	RHP

Table 2

Well	Depth	Sample material	Zircon age	± 2σ	Reference	Petrographic description	Reference	Elemental data for RHP Reference
154/03-1	8060	Core				Amphibolite	Chambers et al. (2005)	Chambers et al. (2005)
164/25-2	8949	Core				Metabasic gneiss	Chambers et al. (2005)	Chambers et al. (2005)
202/02-1	4002	Core	2829	46	Ritchie et al. (2011)	Quartzofeldspathic gneiss	Chambers et al. (2005)	Chambers et al. (2005)
202/03-1	5822	Core				Cataclasite	Chambers et al. (2005)	Chambers et al. (2005)
204/10-1	8199	Core						Finlay et al. (2018)
204/15-2	12467	Cuttings				Tonalite	Finlay et al. (2018)	Finlay et al. (2018)
204/23-1	12622	Core				Quartzofeldspathic gneiss	Chambers et al. (2005)	Chambers et al. (2005)
204/25-1	9417	Core	2729	12	Holdsworth et al. (2019)	Tonalitic gneiss	Chambers et al. (2005)	Chambers et al. (2005)
204/26-1A	8690	Core	2733	14	Holdsworth et al. (2019)	Granodioritic gneiss	Holdsworth et al. (2019)	
204/27a-1	7009	Core	2745	15	Holdsworth et al. (2019)	Granite	Holdsworth et al. (2019)	
204/28-1	6370	Core	2762	13	Holdsworth et al. (2019)	Granodioritic gneiss	Holdsworth et al. (2019)	
205/16-1	13688	Core				Dioritic gneiss	Chambers et al. (2005)	Chambers et al. (2005)
205/20-1	6619	Core	2736	12	Holdsworth et al. (2019)	Granitic gneiss	Holdsworth et al. (2019)	Chambers et al. (2005)
205/21-1A	4449	Core				Granite	Finlay et al. (2018)	Finlay et al. (2018)
205/21-1A	4465	Core				Tonalite	Finlay et al. (2018)	Finlay et al. (2018)
205/22-1A	10747	Core	2700	13	Holdsworth et al. (2019)	Dioritic gneiss	Chambers et al. (2005)	Chambers et al. (2005)
206/08-1a	7567	Core	2691	28	Chemostrat (2014)			

206/08-1A	7582	Core	2801.7	5	Holdsworth et al. (2019)	Dioritic gneiss	Chambers et al. (2005)	Chambers et al. (2005)
206/08-2	6099	Core				Granodiorite	Finlay et al. (2018)	Finlay et al. (2018)
206/08-2	6117	Core				Protomylonite	Chambers et al. (2005)	Chambers et al. (2005)
206/08-7	7613	Core				Amphibolite	Chambers et al. (2005)	Chambers et al. (2005)
206/08-8	8199	Core				Granitic gneiss	Chambers et al. (2005)	Chambers et al. (2005)
206/09-2	8084	Core				Granite/Granite Gneiss	Finlay et al. (2018)	Finlay et al. (2018)
206/12-1	5630	Core				Granodiorite Gneiss	Finlay et al. (2018)	Finlay et al. (2018)
206/12-1	5632	Core	2748	6	Holdsworth et al. (2019)	Granodioritic gneiss	Holdsworth et al. (2019)	
206/7a-2	7023	Core	2809.2	20.83	Chemostrat (2014)			
206/7a-2	7025	Core	2806	8	Holdsworth et al. (2019)	Granodioritic gneiss	Holdsworth et al. (2019)	Chambers et al. (2005)
206/7a-2	8000	Core				Tonalite	Finlay et al. (2018)	Finlay et al. (2018)
206/7a-2	8016	Core				Diorite	Finlay et al. (2018)	Finlay et al. (2018)
206/7a-2	8508	Core	2753	6	Holdsworth et al. (2019)	Granodioritic gneiss	Holdsworth et al. (2019)	Chambers et al. (2005)
206/7a-2	8508	Core	2781.58	24.83	Chemostrat (2014)			
206/7a-2	8528	Core						Chambers et al. (2005)
208/23-1	6795	Core	2776	12	Holdsworth et al. (2019)	Granitic gneiss	Holdsworth et al. (2019)	
208/26-1	12776	Core				Granodiorite	Finlay et al. (2018)	Finlay et al. (2018)
208/27-1	4528	Core	2738.68	22.46	Chemostrat (2014)			
208/27-2	4452	Core	2789	8	Holdsworth et al. (2019)	Mafic-granitic gneiss	Holdsworth et al. (2019)	
208/27-2	4529	Core				Granitic gneiss	Chambers et al. (2005)	Chambers et al. (2005)
209/09-1		Core				Augen gneiss	Chambers et al. (2005)	Chambers et al. (2005)
209/12-1	11526	Core				Biotite schist	Chambers et al. (2005)	Chambers et al. (2005)

214/09-1	15581	Cuttings				Granite	Finlay et al. (2018)	Finlay et al. (2018)
220/26-1		Core				Quartzofeldspathic mylonite	Chambers et al. (2005)	Chambers et al. (2005)

Table 3

Well	Depth (MD; ft)	Material	Data source	K2O (Wt)%	U (ppm)	Th (ppm)	RHP (µWm-3)	Average Well RHP (µWm3)	SD
154/03-1	8060	Core	Chambers et al. (2005)	1.63	0.44	1.76	0.4	0.4	
164/25-2	8949	Core	Chambers et al. (2005)	0.20	0.14	0.15	0.1	0.1	
202/02-1	3950	Cuttings	This Study	1.60	4.56	6.46	1.8	1.3	0.7
	4002	Core	Chambers et al. (2005)	2.19	0.89	6.31	0.9		
202/03-1	5822	Core	Chambers et al. (2005)	1.84	0.10	0.50	0.2	0.2	
202/08-1	5447	Core	This Study	2.75	0.43	0.87	0.4	0.4	0.1
	5457	Core	This Study	1.85	0.22	0.60	0.2		
	5500	Cuttings	This Study	1.90	0.62	1.47	0.4		
	5510	Cuttings	This Study	1.78	1.06	1.78	0.5		
	5520	Cuttings	This Study	1.88	0.73	1.37	0.4		
202/09-1	5379	Core	This Study	0.95	1.17	4.54	0.7	0.7	
204/10-1	8199	Core	Finlay et al. (2018)	2.49	3.17	1.58	1.1	1.0	0.1
	8219	Cuttings	This Study	2.62	2.08	3.46	1.0		
	8228	Cuttings	This Study	2.63	2.15	3.79	1.0		
	8238	Cuttings	This Study	2.48	1.85	3.25	0.9		
	8248	Cuttings	This Study	2.64	1.88	3.64	1.0		
204/15-2	12467	Cuttings	Finlay et al. (2018)	0.70	0.27	0.38	0.2	0.2	
204/23-1	12622	Core	Chambers et al. (2005)	1.93	0.69	4.40	0.6	0.6	
204/25-1	9417	Core	Chambers et al. (2005)	1.37	0.07	0.09	0.1	0.1	
205/16-1	13688	Core	Chambers et al. (2005)	3.77	0.54	10.90	1.2	1.0	0.5
	14023	Core	This Study	1.72	0.58	9.36	1.0		
	14024	Core	This Study	1.78	0.39	2.43	0.4		
	14027	Core	This Study	1.59	0.61	28.62	2.4		
	14039	Core	This Study	1.69	0.51	7.69	0.8		
	14108	Cuttings	This Study	2.90	0.50	8.37	1.0		
	14124	Cuttings	This Study	3.32	0.42	7.46	0.9		
	14140	Cuttings	This Study	3.42	0.31	7.57	0.9		
	14154	Cuttings	This Study	3.47	0.29	4.57	0.7		
205/21-1A	4449	Core	Finlay et al. (2018)	0.62	0.35	0.11	0.1	0.1	0.0
	4465	Core	Finlay et al. (2018)	0.66	0.34	0.12	0.1		
205/22-1A	10747	Core	Chambers et al. (2005)	8.36	0.20	0.70	0.7	0.7	
206/08-1A	7582	Core	Chambers et al. (2005)	2.97	0.70	3.20	0.6	1.5	
206/08-2	6099	Core	Finlay et al. (2018)	3.80	7.11	1.66	2.3	2.1	0.2
	6117	Core	Chambers et al. (2005)	0.89	1.03	21.80	1.9		
206/08-7	7613	Core	Chambers et al. (2005)	0.97	0.89	5.02	0.7	0.5	
206/08-8	8199	Core	Chambers et al. (2005)	2.16	0.24	0.32	0.2	1.5	

206/09-2	8084	Core	Finlay et al. (2018)	7.62	7.77	1.00	2.7	1.6	
206/12-1	5630	Core	Finlay et al. (2018)	2.69	0.88	0.18	0.4	0.7	
206/7a-2	7025	Core	Chambers et al. (2005)	2.69	1.12	5.66	0.9	0.6	0.4
	7043	Core	This Study	1.19	0.36	0.39	0.2		
	7047	Core	This Study	1.33	0.59	0.54	0.3		
	7370	Core	This Study	1.72	0.50	10.94	1.1		
	8000	Core	Finlay et al. (2018)	1.24	1.84	0.35	0.6		
	8014	Core	This Study	1.18	0.59	3.81	0.5		
	8015	Core	Finlay et al. (2018)	1.24	1.84	0.35	1.7		
	8016	Core	This Study	1.26	0.45	3.08	0.4		
	8223	Core	This Study	6.34	0.20	0.18	0.5		
	8345	Core	This Study	1.13	0.38	1.01	0.3		
	8508	Core	This Study	2.47	0.55	0.88	0.4		
	8517	Core	This Study	6.17	0.33	0.61	0.6		
	8524	Core	This Study	4.87	0.33	1.08	0.5		
	8528	Core	Chambers et al. (2005)	4.39	0.14	0.76	0.4		
207/01-3	4576	Core	This Study	3.85	0.68	6.53	0.9	1.1	0.2
	4670	Cuttings	This Study	3.03	0.68	9.60	1.1		
	4680	Cuttings	This Study	3.11	0.72	6.46	0.9		
	4690	Cuttings	This Study	2.88	0.56	14.20	1.4		
	4700	Cuttings	This Study	3.15	0.62	8.70	1.0		
	4706	Cuttings	This Study	3.13	0.61	8.38	1.0		
207/02-1	6722	Core	This Study	6.52	0.63	1.47	0.8	0.8	0.1
	6723	Core	This Study	6.67	0.69	1.23	0.8		
	6724	Core	This Study	6.46	0.78	2.48	0.9		
208/23-1	6796.6	Core	This Study	4.52	0.94	15.72	1.7	1.2	0.7
	6799	Core	This Study	2.81	0.63	2.51	0.6		
	6803	Core	This Study	3.66	0.63	0.98	0.5		
	6806	Core	This Study	4.99	0.80	19.07	2.0		
	6808	Core	This Study	6.81	0.83	5.12	1.1		
208/26-1	12776	Core	Finlay et al. (2018)	1.47	0.34	0.09	0.2	0.3	
208/27-2	4522	Core	This Study	2.58	0.48	0.36	0.3	0.6	0.3
	4527.5	Core	This Study	2.24	1.42	2.72	0.7		
	4529	Core	Chambers et al. (2005)	3.39	1.61	4.92	1.0		
	4531	Core	This Study	3.17	0.31	0.69	0.4		
	4532	Core	This Study	2.59	0.94	0.65	0.5		
209/09-1		Core	Chambers et al. (2005)	4.55	0.62	6.80	1.0	1.0	0.5
	8850	Core	This Study	3.63	3.12	11.76	1.9		
	8854	Core	This Study	2.73	3.65	9.84	1.9		
	8855	Core	This Study	3.49	2.36	5.77	1.3		
209/12-1	11386	Core	This Study	2.07	11.03	7.59	3.6	2.4	0.6
	11500	Core	This Study	3.70	4.61	8.25	2.1		
	11510	Cuttings	This Study	3.80	4.49	9.93	2.2		
	11520	Cuttings	This Study	4.07	4.13	10.44	2.1		
	11525	Cuttings	This Study	3.69	2.03	17.41	2.1		
	11526	Core	Chambers et al. (2005)	3.93	2.50	23.80	2.7		
	11527	Cuttings	This Study	5.64	2.32	17.45	2.3		
214/09-1	15581	Cuttings	Finlay et al. (2018)	4.63	7.92	1.51	2.5	1.7	

220/26-1		Core	Chambers et al. (2005)	2.28	1.54	5.10	0.9	0.9	

Table 4

Well	Depth (ft)	Sample material	Petrographic technique	Texture	QAP designation	Description	Data source
202/08-1	5447	Core	Thin Section	Gneissic	Monzodiorite		This study
202/08-1	5457	Core	Thin Section	Gneissic	Tonalite		This study
202/08-1	5500	Cuttings	XRD	Gneissic	Granodiorite		This study
202/08-1	5510	Cuttings	XRD	Gneissic	Granodiorite		This study
202/08-1	5520	Cuttings	XRD	Gneissic	Granodiorite		This study
202/09-1	5379	Core	Thin Section	Gneissic	Monzodiorite		This study
205/16-1	14023	Core	Thin Section	Gneissic	Granodiorite		This study
205/16-1	14024	Core	Thin Section	Gneissic	Granite - Granodiorite		This study
205/16-1	14027	Core	Thin Section	Gneissic	Granite - Granodiorite		This study
205/16-1	14039	Core	Thin Section	Gneissic	Tonalite		This study
205/16-1	14108-14154	Cuttings	XRD	Gneissic	Granite - Granodiorite		This study
206/7a-2	7043	Core	Thin Section	Gneissic	Granodiorite		This study
206/7a-2	7047	Core	Thin Section	Gneissic	Tonalite		This study
206/7a-2	7370	Core	Thin Section	Gneissic	Granodiorite		This study
206/7a-2	8014	Core	Thin Section	Gneissic	Quartz Diorite		This study
206/7a-2	8016	Core	Thin Section	Gneissic	Tonalite		This study
206/7a-2	8223	Core	Thin Section	Gneissic	Tonalite		This study
206/7a-2	8345	Core	Thin Section	Gneissic	Tonalite		This study
206/7a-2	8508	Core	Thin Section	Gneissic	Granite		This study
206/7a-2	8517	Core	Thin Section	Gneissic	Tonalite		This study
206/7a-2	8524	Core	Thin Section	Gneissic	Tonalite		This study
207/01-3	4576	Core	Thin Section	Schistose	N/A		This study
207/01-3	4670-4706	Cuttings	XRD	Gneissic	Granodiorite		This study
207/02-1	6722	Core	Thin Section	Gneissic	Granite		This study
207/02-1	6723	Core	Thin Section	Gneissic	Granite		This study
207/02-1	6724	Core	Thin Section	Gneissic	Granite		This study

208/23-1	6797	Core	Thin Section	Gneissic	Qtz ritch granitoid		This study
208/23-1	6799	Core	Thin Section	Gneissic	Granite		This study
208/23-1	6803	Core	Thin Section	Gneissic	Qtz ritch granitoid		This study
208/23-1	6806	Core	Thin Section	Gneissic	Granite		This study
208/23-1	6808	Core	Thin Section	Gneissic	Granite		This study
209/09-1	8850	Core	Thin Section	Plutonic	Granodiorite		This study
209/09-1	8854	Core	Thin Section	Plutonic	Granodiorite		This study
209/09-1	8855	Core	Thin Section	Plutonic	Qtz ritch granitoid		This study
209/12-1	11500	Core	Thin Section	Plutonic	Granite		This study
209/12-1	11510	Core	Thin Section	Plutonic	Alkali-feldspar Granite		This study
209/12-1	11520-11527	Cuttings	XRD	Plutonic	Granite		This study
204/26-1A	8690	Core				Granodioritic gneiss	Holdsworth et al. (2019)
204/27a-1	7009	Core				Granite	Holdsworth et al. (2019)
204/28-1	6370	Core				Granodioritic gneiss	Holdsworth et al. (2019)
205/20-1	6619	Core				Granitic gneiss	Holdsworth et al. (2019)
206/12-1	5632	Core				Granodioritic gneiss	Holdsworth et al. (2019)
206/7a-2	7025	Core				Granodioritic gneiss	Holdsworth et al. (2019)
206/7a-2	8508	Core				Granodioritic gneiss	Holdsworth et al. (2019)
208/23-1	6795	Core				Granitic gneiss	Holdsworth et al. (2019)
208/27-2	4452	Core				Mafic-granitic gneiss	Holdsworth et al. (2019)
204/15-2	12467	Cuttings			Tonalite		Finlay et al. (2018)
205/21-1A	4449	Core			Granite		Finlay et al. (2018)
205/21-1A	4465	Core			Tonalite		Finlay et al. (2018)
206/08-2	6099	Core			Granodiorite		Finlay et al. (2018)
206/09-2	8084	Core			Granite		Finlay et al. (2018)
206/12-1	5630	Core			Granodiorite		Finlay et al. (2018)
206/7a-2	8000	Core			Tonalite		Finlay et al. (2018)
206/7a-2	8016	Core			Diorite		Finlay et al. (2018)

208/26-1	12776	Core			Granodiorite		Finlay et al. (2018)
214/09-1	15581	Cuttings			Granite		Finlay et al. (2018)
154/03-1	8060	Core				Amphibolite	Chambers et al. (2005)
164/25-2	8949	Core				Metabasic gneiss	Chambers et al. (2005)
202/02-1	4002	Core				Quartzofeldspathic gneiss	Chambers et al. (2005)
202/03-1	5822	Core				Cataclasite	Chambers et al. (2005)
204/23-1	12622	Core				Quartzofeldspathic gneiss	Chambers et al. (2005)
204/25-1	9417	Core				Tonalitic gneiss	Chambers et al. (2005)
205/16-1	13688	Core				Dioritic gneiss	Chambers et al. (2005)
205/22-1A	10747	Core				Dioritic gneiss	Chambers et al. (2005)
206/08-1A	7582	Core				Dioritic gneiss	Chambers et al. (2005)
206/08-2	6117	Core				Protomylonite	Chambers et al. (2005)
206/08-7	7613	Core				Amphibolite	Chambers et al. (2005)
206/08-8	8199	Core				Granitic gneiss	Chambers et al. (2005)
208/27-2	4529	Core				Granitic gneiss	Chambers et al. (2005)
209/09-1		Core				Augen gneiss	Chambers et al. (2005)
209/12-1	11526	Core				Biotite schist	Chambers et al. (2005)
220/26-1		Core				Quartzofeldspathic mylonite	Chambers et al. (2005)

Table 5

Well	Depth (ft)	Sample material	Age (Ma)	± 2σ	MSWD	Data source
204/10-1	8219-8248	Cuttings	Insufficient zircons recovered to produce an age			This study
205/16-1	14027	Core	2738.3	6	4	This study
205/16-1	14108-14154	Cuttings	2742.0	6	4.9	This study
206/7a-2	7047	Core	2851.0	18	30	This study
206/7a-2	8524	Core	2726.0	8	3.7	This study
207/01-3	4670-4706	Cuttings	2734.0	16	25.0	This study
207/02-1	6722	Core	2732.0	4	3.0	This study
207/02-1	6723	Core	2735.0	5	4.4	This study
207/02-1	6724	Core	2735.0	4	3.1	This study
208/23-1	6797	Core	2782.5	6	6.0	This study
208/27-2	4528	Core	2742	6	11.0	This study
209/09-1	8854	Core	463.0	6.0	2.8	This study
202/02-1	4002	Core	2829	46		Ritchie et al. (2011)
204/25-1	9417	Core	2729	12		Holdsworth et al. (2019)
204/26-1A	8690	Core	2733	14		Holdsworth et al. (2019)
204/27a-1	7009	Core	2745	15		Holdsworth et al. (2019)
204/28-1	6370	Core	2762	13		Holdsworth et al. (2019)
205/20-1	6619	Core	2736	12		Holdsworth et al. (2019)
205/22-1A	10747	Core	2700	13		Chambers et al. (2005)
206/08-1A	7582	Core	2801.7	5		Chambers et al. (2005)
206/12-1	5632	Core	2748	6		Holdsworth et al. (2019)
206/7a-2	7025	Core	2806	8		Holdsworth et al. (2019)
206/7a-2	8508	Core	2753	6		Holdsworth et al. (2019)
208/23-1	6795	Core	2776	12		Holdsworth et al. (2019)
208/27-2	4452	Core	2789	8		Holdsworth et al. (2019)
206/08-1a	7567	Core	2691	28	15	Chemostrat (2014)

206/7a-2	7023	Core	2809.2	21	6.3	Chemostrat (2014)
206/7a-2	8508	Core	2781.58	25	11	Chemostrat (2014)
209/12-1	11521	Core	423	20	1.9	Chemostrat (2014)